Fachtagung “Experimentelle Strömungsmechanik”
6.–8. September 2022, Ilmenau

Druckkraftantwort auf eine Kugel bei instationärer Anströmung mit sinusartigem Seitenwind

PRESSURE FORCE RESPONSE ON A SPHERE IN UNSTEADY FLOW WITH SINUSOIDALLY ALTERNATING CROSSWIND

Max Müller[1], Klaus Ehrenfried[1], Claus Wagner[1,2]
[1] DLR - Insitute of Aerodynamics and Flow Technologies – Ground Vehicles, Bunsenstraße 10, 37073 Göttingen
[2] TU Illmenau – Fakultät Maschinenbau – FG Aerodynamik – Am Helmholtzring 1, 98693 Ilmenau

Druckkraftantwort, Admittanz, instationäre Anströmung
pressure force answer, admittance, unsteady inflow

Summary

The response forces on a sphere in sinusoidal cross winds with frequencies between 20 Hz and 50 Hz and small amplitudes (<3°) derived from surface pressure measurements have been investigated in wind tunnel experiments. Two different undisturbed inflow velocities were considered, which lead to a sub- and a supercritical flow separation pattern. The amplitude of the side force response was found to depend linearly on the amplitude of the inflow angle and grows non-linearly with increasing reduced frequency. The phase angle between inflow and side force response increases linearly with the reduced frequency. Both the amplitude and the phase angle of the side force response collapse on a single trend for the sub- and supercritical flow separation, hence the trend is only a function of the reduced frequency. Calculating a virtual point of force application, where the force is in phase with the inflow angle, it was shown that this point is independent of the reduced frequency.

Introduction

Ground-based vehicles are exposed to transient inflow conditions during their operation. The inflow conditions are generated by other road users, eg. during over taking, close objects like signs and trees, or simply gusty wind and side wind conditions. Especially the latter directly influences the side wind stability of cars, as well as trains. In order to ensure safety and comfort of ride, it is important to be able to predict the force answer to transient inflow conditions, so that the force response can already be considered during the design phase of ground-based vehicles. For this purpose, transfer functions are used, which describe the amplitude of the force response and phase to the inflow as a function of the reduced frequency of the inflow.
However, for ground-based vehicles often only the amplitude of the response force as function of the reduced frequency is of interest. Schröck 2011, for example, studied the impact of the driver’s counter-steering and response time. He determined the amplitude of the force response for certain critical frequencies, by using the aerodynamic admittance function, which connects the power spectrum of the inflow with the response force´s power spectrum. The same definition of aerodynamic admittance is often used for trains, concerning safety issues, as for example overturning due to sudden gusts. Since there are multiple reports on the

admittance for various train designs, obtained from full scale on-rail measurements, as well as wind tunnel testing, Sterling et al. 2009 looked for commonalities in the aerodynamic admittance functions. Comparing the admittance functions of side and lift force from the different measurements, they conclude all the admittances collapse on a single curve, if adjusted properly, despite significant scattering. However, concerning the lift admittance, the full-scale data and the wind tunnel data needed to be treated separately, because of systematic differences. They assumed that some sort of vortex induced phenomenon on the roof of the train, which occurs in full-scale, but not in wind tunnel testing was responsible for the differences.
However, using the energy spectra of the response force and inflow, they lost the information on the phase between the gust and the response force due to the squaring of the spectra in the frequency domain. Though, from early investigations on the force answers on transient inflow, like the one of Sears 1941, who investigated the lift on an airfoil in sinusoidal inflow with different reduced frequencies, it is known that the phase angle is also a function of the reduced frequency. In contrast to the aforementioned studies on ground-based vehicles, Sears 1941 aimed at a transfer function, including amplitude and phase to the inflow. Such a transfer function also allows to superimpose different frequencies in the inflow.
In order to engage a transfer function, which reflects the conditions of wind tunnel testing with transient inflow regarding ground-based vehicles, the response forces on a sphere are considered in this work. The geometrical simple sphere was chosen as a model to avert geometrical influences and because of its radial symmetry. Landau and Livshitz 1959, were able to derive equation 1 from potential theory, to describe the forces on a sphere, with oscillatory conditions.

$$F = 6\pi\mu a U_0 e^{-i\omega t}\left[1 + (1-i)\left({\omega a^2}/{2\nu}\right)^{\frac{1}{2}} - i\frac{2}{9}{\omega a^2}/{2\nu}\right] \tag{1}$$

Where a denotes the radius of the sphere, ν and μ the kinematic and dynamic viscosity respectively, ω the oscillation frequency and U_0 the velocity. Furthermore, equation 1 reflects three terms. The first term describes the quasi-steady drag. The second term is also known as Basset force and reflects changes in the boundary layer that lead to varying shear stress. The third term corresponds to the acceleration of the displaced volume and is named added mass term. It must be noted that the last two terms lead to a phase shift between inflow and force response and also include the dependency of the force amplitude on the frequency. However, because the equation is derived from potential theory it is only valid for small Reynolds numbers. At higher Reynolds numbers, the flow separation from the sphere switches from laminar to turbulent, as described by Prandtl 1914. When approaching a critical Reynolds number of $Re_{D,crit} \approx 3x10^5$ the boundary layer becomes turbulent upstream the separation line, leading to an abrupt leeward shift of the line of separation. This results in a smaller a detached area and therefore lower drag.
In this work, the side force response on a sphere mounted on a cross stream rod (CSR) in sinusoidal crosswinds was examined for two inflow velocities, which are connected to a sub and a super-critical Reynolds number. The amplitude of the side force and the phase to the inflow oscillation are presented as function of the reduced frequency.

Experimental set-up

The wind tunnel experiments were performed in the side wind facility Göttingen (SWG). The SWG is a closed-circuit wind tunnel with a closed test section, which is 9 m long, 2.4 m wide and 1.6 m high. The maximum wind speed is u_0 = 65 m/s at a degree of turbulence of less than Tu ≤ 0.25%.

A gust generator consisting of four wings with a NACA 0018 profile and movable flaps is installed at the beginning of the test section and generates the sinusoidal inflow field. The setup is shown schematically in Figure 1, where the undisturbed inflow with the velocity u_0 approaches from the left and passes the gust generator. The wings with the NACA 0018 profile have a chord length of c = 0.3 m and a span of 0.8 m. Since this is only half of the height of the test section, the gust generator can also be used for inducing low frequencies. The transient inflow is generated by the movable flaps with a length of 1/3c, which are represented in black. Each flap is movable by a separate servo drive. The spacing between the two center wings is enhanced to avoid interaction of the wing´s wakes and the flow around the sphere.
The center of the sphere is placed 5c downstream of the flaps trailing edges. The diameter of the sphere is D = 120 mm, and it is mounted on a vertical cross-stream rod (CSR) with a diameter of 25 mm. The CSR is connected to a turn table outside of the wind tunnel. The sphere has eight pressure taps, which are positioned as shown in Figure 1 right, on four different colatitudes Θ = 20°, 60°, 100°, 140°. In order to obtain 48 facets, each experiment was conducted six times for different azimuthal angles φ = 90°, 60°, 30°, 0°, -30°, -60°, which were set with the turn table. The different measurements were later synchronized, using the signal of the flap's servo drive resolver. As a result, the sphere is virtually facetted as shown in Figure 1 right. The pressure transducers were put as near as possible to the pressure measurement hole in order to avoid any damping, which still leads to a distance of 400 mm. A tube with an inner diameter of 1 mm connects the pressure measurement hole with a diameter of 1 mm and the piezoresistive pressure transducer ENDEVCO 8510-B2.
Parallel to the center of the sphere was a two-hole probe to obtain a signal of the inflow angle. The dynamic pressures of the two holes of the two-hole probe were measured with two ENDEVCO 8507-C2.

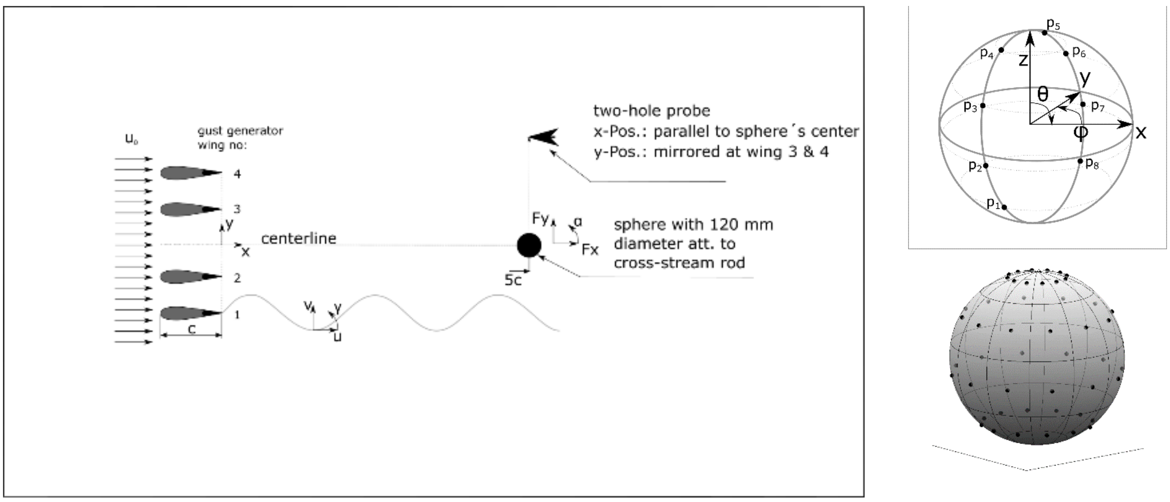

Fig. 1: Schematic representation of the test set up: left: set up in the test section of the wind tunnel, right) coordinate system for the sphere and the resulting 48 facets

The signals of the pressure transducers in the sphere and of the two-hole probe, as well as the signal of the servo drive were recorded with a DEWETRON 501 at a sample rate of 1 kHz, a duration of 25 s and a resolution of 24 bit.
The experiments were conducted for two different wind speeds u_0 = 30 m/s and u_0 = 50 m/s resulting in a case, where the flow separation on the sphere is supposedly laminar (subcritical) and one with turbulent flow separation (supercritical). For both wind speeds, the amplitude for the flap movement was set to 1°, 2° and 3°. Six different gust frequencies were investigated: f_{gust} = 20 Hz, 25 Hz, 30 Hz, 40 Hz, 45 Hz, 50 Hz. The resulting reduced frequencies, build with

the natural frequency $k = {}^{Df_{gust}}/_{u_0}$ were accordingly in the range of $0.048 \leq k \leq 0.2$. This definition of the reduced frequency can be thought of as a ratio of the length scale of the model and the wavelength of the gust, where k = 0.2 is equivalent to a wave length equal to five times the diameter of the sphere. In airfoil aerodynamics reduced frequencies are often defined, like for example by Sears 1941, as, $k_{foil} = {}^{c_{foil}\omega_{gust}}/_{u_0}$. Following this definition $k_{foil} > 0.05$ is considered unsteady, while $k_{foil} > 0.2$ is called highly unsteady. By building the reduced frequency accordingly, with the sphere diameter instead of the chord length, it is seen that the range of reduced frequencies in this work is considered highly unsteady ($k_{foil,D} > 0.3$).

Methodology of calculating the response force

Wind induced forcing is not only a problem to ground-based vehicles, but also to high slender buildings, where the wind loads induce vibrations of the building. Wind induced forces are often measured by integrating the surface pressure, as done by Rosa et al. 2012, who investigate the interaction of the mechanical vibration modes and the forces obtained at different heights on a rigid model in wind tunnel testing. The main objective is similar to the measurement of unsteady forces on ground-based vehicles, which is to ensure safety and comfort at an early level of the design. Concerning ground-based vehicles Schröck and Wagner 2013 state that the kinetic energy of transient inflow translates to surface pressures, also reflecting local phenomena. Additionally, it is stated that the response force can be deduced from the pressure amplitude, when the phase information of the different pressure taps is included.
In Figure 2 left, the frequency spectra of one pressure tap and the flow angle measured at the two-hole probe are presented. For this example, the measurement setting with u_0 = 30 m/s, β_{flap} = 2°, f_{gust} = 30 Hz, Θ = 210° and φ = 100° was chosen. The frequency spectrum was transformed into decibel to highlight the peaks. The upper graph shows the frequency spectrum of the pressure tap, showing a sharp peak at the excitation frequency of f_{gust} = 30 Hz, while the narrowness of this peak implies low damping. The other peaks, like those of added harmonics, are multiple orders of magnitude smaller. The same is seen for the flow angle γ signal, which was deduced from the two-hole probe and is displayed below the surface pressure tap signal.
In Figure 2 right, the maximum of the cross-correlation of the pressure signals and the signal of the flaps is shown in a polar plot. According to the set coordinate system (compare Figure 1), the polar plot can be thought of as top view on the sphere, with the flow approaching from the left-hand side. The azimuthal angle and the correlation coefficient define the coordinate system for the four graphs representing the colatitudes. The cross-correlation coefficient was calculated according to equation 2.

$$r(\tau) = \frac{cov(p(\tau : 25s - \mathrm{T} + \tau), \measuredangle(0.001s : 25s - \mathrm{T}))}{\sigma_{p_i}\sigma_{\measuredangle}} \qquad (2)$$

The pressure signal was shortened by a period $T = 1/f_{gust}$ and subsequently a time parameter τ shifts the pressure signal in relation to the flap angle signal. Consequently, a cross-correlation over the period T is found for each pressure tap. Its maximum gives insight into the spatial excitement of the surface pressure by the sinusoidal inflow. It can be seen, that the cross-correlation is maximal at the azimuthal angle φ = 150° and φ = 210° for each colatitude, whereas in the wake region the pressures are decorrelated from the flap angle. Also, the pressure taps of the colatitude Θ = 20° are decorrelated from the flap movement and subsequently from the inflow angle. This shows that the response force to the gust is mainly reconstructed from three colatitudes and five different azimuthal angles. Additionally, the linear connections between the maximal correlation coefficients in Figure 2 right show sharp angles, from which it is concluded that this spatial resolution leads to inaccuracies in the numerical integration to obtain the force. Accordingly, a higher spatial resolution would be desirable, which comes with the cost of a higher number of experiments and was therefore not possible. However, the pressure force response calculated this way should be sufficient to describe the trend of the force response as function of the reduced frequency.

Noteworthy, there is peak at the azimuthal angle φ = 60°. This peak is due to the preferred deflection direction of the bistable wake, which is known for a sphere on CSR, as shown by Müller et al. 2019 in wind tunnel testing and by Bauer et al. 2021 analyzing Large-Eddy Simulation performed with a Lattice-Boltzmann method. Anyway, the low frequency side force behavior, including bistability, is not part of this work.

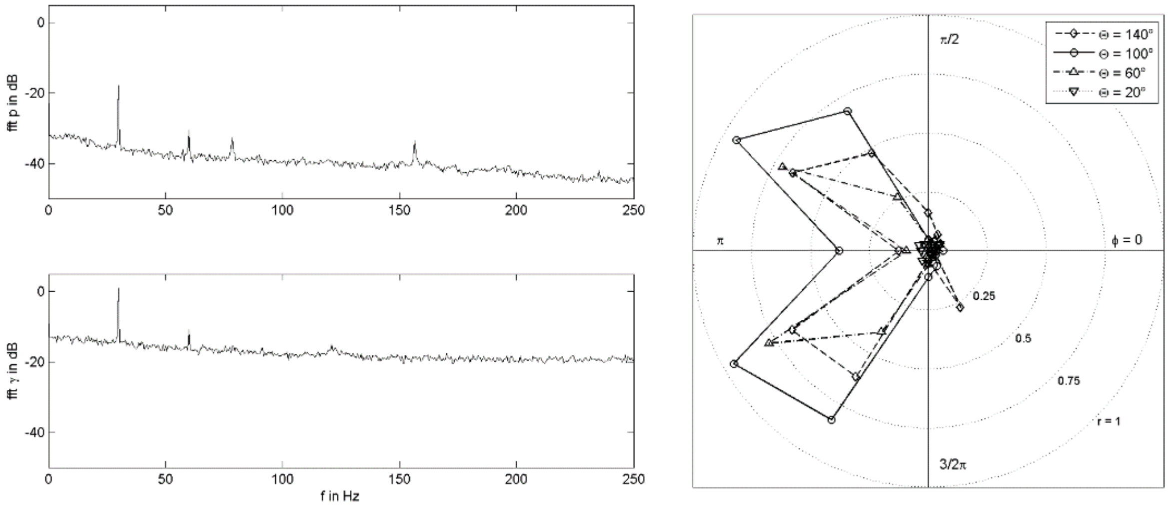

Fig. 2: Measurement series u_0 = 30 m/s, β_{flap} = 2°, f_{gust} = 30 Hz, left, top: frequency spectrum at pressure tap Φ = 210°, Θ = 100° in dB; left, bottom: frequency spectrum of the inflow angle γ in dB, measured with the two-hole probe; right: polar plot of the maximal cross correlation coefficient for all pressure taps

Since the 48 facets discretizing the sphere result from six measurements with the same set up of u_0, f_{gust} and β, but different azimuthal angle φ, the time lines of the surface pressures need to be synchronized with respect to the flow angle. This is achieved by using the flap movement signal as reference. In order to calculate the force connected to the excitation frequency, the pressure amplitude at the gust frequency and the phase to the flap movement were derived from the frequency spectrum. The found pressure amplitudes and phases, are then transformed to forces, by using the area of the facets, shown in Figure 1 right and the direction of the force is retrieved directly from the angles Θ and φ. By adding up the forces of each facet, the amplitude of the response force and the phase to the flap movement for the whole sphere is obtained for each setting of u_0, f_{gust} and β. The side force is then normalized to a side force coefficient $c_S = \frac{2F_S}{\rho {u_0}^2 A}$, with F_s being the side force, A denotes the projection area of the sphere and ρ the density of the fluid.

Amplitude of the force response and phase against flap signal

The amplitude of the side force coefficient has been normalized by the flow angle γ to $\zeta = c_S/\gamma$. This is done because the flow angle γ itself is a function of the amplitude of the flap movement β and the reduced frequency of the flap. Mullarkey 1990 found that this behavior could be modelled by discretizing the flap movement and at each time step a line vortex is shed at the trailing edge into the wake, which is then convected with the flow. The vortex-vortex interaction during the convection leads to a good approximation of the induced flow angle at the model position downstream the gust generator. The normalized amplitude ζ is plotted against the reduced frequency in Figure 3 left. Due to the normalization the normalized amplitudes collapse to a single point, with some scatter, which highlights that the side force coefficient amplitude is directly proportional to the inflow angle amplitudes. The scatter can be minimized, by increasing the spatial resolution of facets, or the number of pressure taps. In addition, it must be mentioned that the measurement of u_0 = 50 m/s, β_{flap} = 1°, f_{gust} = 30 Hz was excluded because of a measurement error for one of the azimuthal angles.

Besides the observation that the influence of the amplitude of the inflow angle γ can be regarded linear, Figure3 left shows that for low reduced frequencies, the normalized amplitude of the side force coefficient is slightly smaller than $\zeta = c_S/\gamma \approx 0.009$, whereas for higher reduced frequencies the normalized amplitude rises non-linearly.
Additionally, it can be depicted that the normalized amplitudes collapse to a single trend for sub- and supercritical flow separation. Whether this observation for a sphere mounted on CSR can transferred to a plain sphere is not clear. Figure 2 shows that the area of high correlation between pressure signal and flap movement is distinct from the area of flow separation. Since the two effects act on different locations they may not have a strong influence on each other. However, there is another possible explanation. The supercritical flow separation on a plain sphere goes along with a smaller area of flow separation compared to the subcritical flow separation, leading to a so called drag crisis. However, Bauer et al. (2021) have shown in agreement from simulation and experiment that there is no such drag crisis for this experimental set up of a sphere mounted on a CSR. The interaction of the wake of the CSR and the sphere cause that the supercritical wake does not shrink, as it would without the lateral model mount. This makes the detached area similar for the sub- and supercritical case and thus results in a similar pressure regain and consequently drag coefficient. Concluding, there is the possibility that the course of the normalized amplitudes is the same for sub- and supercritical separation, because the flow separation pattern is not differing much due to the CSR.

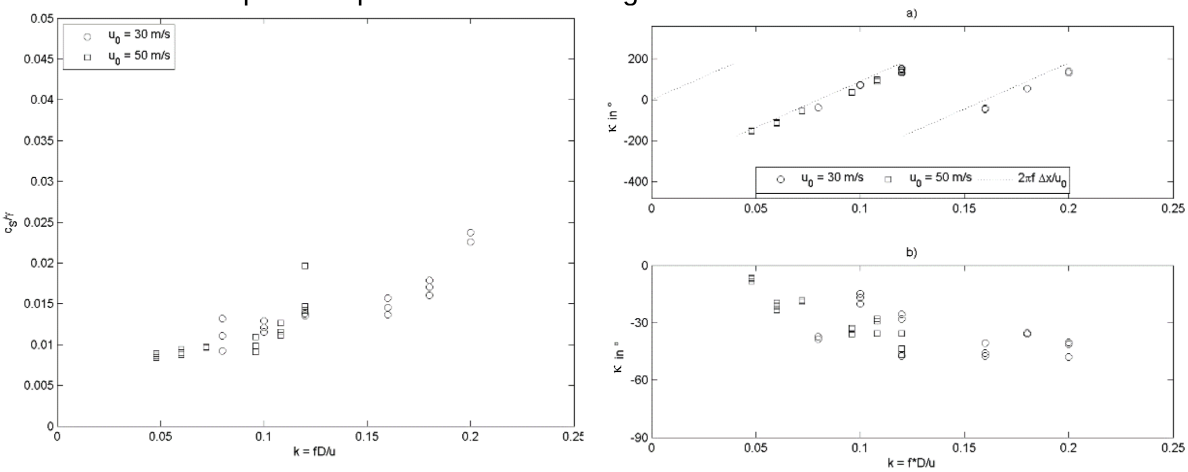

Fig. 3: Left: amplitude of the side force coefficient normalized with the inflow angle amplitude; right a): phase between flap movement and response force with convected gust (dashed line); right b) phase angle between theoretical convected gust and response force

In Figure 3 right a) the phase between the flap movement and the force response is plotted. Additionally, a dotted line simulates the effect of line vortices shed at the trailing edge of the flaps, which are then convected with the undisturbed inflow velocity u_0. Since the line vortices are the cause of the induced flow angle, the convection model of the vortices also reflects the phase between the theoretical flow angle at the center of the sphere to the signal of the flap movement, and can be derived from $\kappa_{konv} = 360°f\ 5c/u_0$. It is seen that the phase angle between side force coefficient timeline and the timeline of the flap movement κ_{force} at certain reduced frequency is always smaller than the phase angle between the theoretical inflow angle and the flapmovement κ_{konv}. This is highlighted by plotting the difference between the phase angles κ_{konv} and κ_{force}, which is shown in Figure 3 right b, reflecting that the lag between force and inflow increases with the increase of the reduced frequency.

Phase between force and inflow

It is known from Mullarkey 1990 that the convection velocity of the induced gust is not sufficiently expressed by the undisturbed inflow velocity u_0. Because of the lower wind speed in the wing´s wakes and vortex-vortex interaction of the shed line vortices the resulting convection velocity is also function of the reduced frequency. Hence, prior to installing the sphere in the test section, a pretest was undertaken with the two-hole probe positioned at the later center of the sphere. By doing so, the phase between flap movement and the flow angle at the position of the center of the sphere was determined directly. The results of this pretest were considered for the phase between inflow and side force coefficient, the course of which is plotted in Figure 4 a). Here, for very small frequencies the phase lag is nearly 0, as expected, since the response force is in phase with quasi steady changes of the inflow angle. This also fits to equation 1, where the quasi steady term does not reflect any phase lag. The linear fit highlights the direct proportionality, which is now apparent in comparison to Figure 3 right b), despite some scatter. The phase between the side force signal and the oscillatory inflow was derived from their time-lines. Another way to access the phase is related to the spatial progression of the gust. Therefore, a virtual point of force application has been calculated, at which the side force coefficient timeline and the inflow angle timeline are in phase. The position has been determined in relation to the center of the sphere ($x_{center} = 0$) and has also been normalized by the radius of the sphere R, according to equation 3.

$$x(k) = \frac{\kappa(k)}{360°}\frac{u_0}{f_{gust}}\frac{1}{R} \qquad (3)$$

In Figure 4 b) the location of the virtual point of force application is shown to scatter around the rear of the sphere. The linear fit reveals that the point of force application does not change with the reduced frequency and is also not depend on, whether the flow separation is sub- or supercritical. Because the location of the virtual point of force application x was found to be constant in the range of $0.048 \leq k \leq 0.2$, it can be determined from one single measurement. Additionally, the course of the phase angle κ between the side force coefficient timeline and the inflow angle timeline is a function of the induced wavelength $\lambda = u_0/f_{gust}$ and can be calculated from equation 4.

$$\kappa(k) = {}^{Rx}/_{\lambda}\, 360° \qquad (4)$$

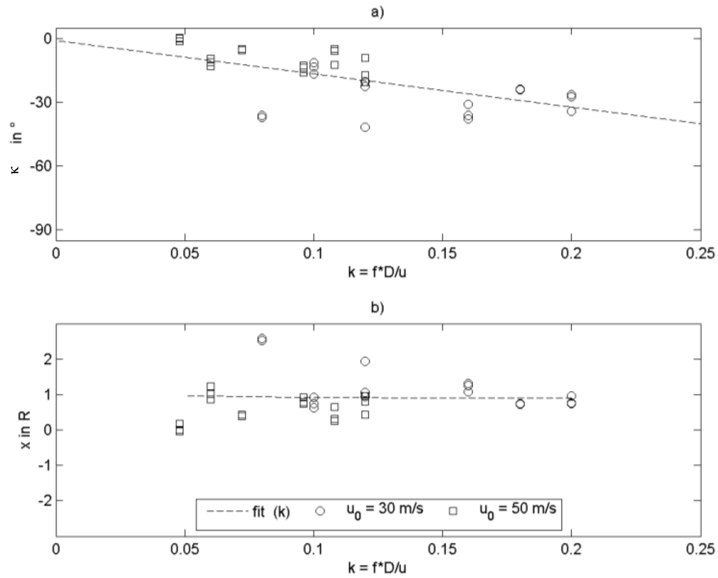

Fig. 4: a) Phase angle κ with the corrected phase of the approaching flow angle; b) virtual point of force application as function of the reduced frequency

Conclusions and perspectives

The surface pressure on a sphere in sinusoidal crosswinds was measured to determine the amplitude and phase of the side force response for two inflow velocities, for which a sub- and a supercritical flow around the sphere was observed. It is found that the amplitude of the side force coefficient is directly proportional to small amplitudes of the sinusoidal inflow angle.

Furthermore, it rises non-linearly with the reduced frequency. The trend for the amplitude of the side force coefficient over the reduced frequency appears to collapse to a single trend for both undisturbed inflow velocities reflecting the sub- and supercritical flow separation. The linear trend of the phase angle between force and inflow was derived by including more precise information on the convection of the induced flow angle. By calculating a virtual point of force application with zero phase, it is shown that this point does not depend on the reduced frequency. Furthermore, the phase angle can be interpreted as ratio of the distance between the center of the sphere and the virtual point of force application to the wavelength of the induced sinusoidal cross wind.

With the graphs shown in Figure 3 left and Figure 4 a) the transfer function for the response force to a sinusoidal inflow could be written like in equation 5.

$$c_S(k,t) = \gamma_{amp}\zeta(k)\sin(2\pi f_{gust}t + \kappa(k)) \tag{5}$$

The fact that the different flow patterns belonging to the sub- and supercritical flow separation did not directly affect the amplitude of the side force coefficient might have to do with the lack of a drag crisis for a sphere on cross-stream rod, as described by Bauer et al. 2021. In order to allow the drag crisis to appear further numerical simulations on a sphere in sinusoidal cross-winds without model mount need to be investigated in future work. Furthermore, the area, where the impact of the transient inflow is the highest, is distinct from the area of separation and the area of lowest static pressure. This means that changes in the flow patterns there might not alter the response force to sinusoidal inflow.

Literature

Bauer C., Müller M., Ehrenfried K., Wagner C., 2021: “Bi-stability detection in the flow around a sphere by means of experiments and lattice Boltzmann simulations” New Results in Numerical and Experimental Fluid Mechanics XIII. pp 441-450

Landau, L.E., Livshitz, E.M., 1959: "Fluid Mechanics", Oxford, Pergamon Press

Mullarkey, P.S. 1990: „Aerodynamic stability of road vehicles in side winds and gusts”, PhD Thesis Imperial College London

Müller, M., Ehrenfried, K., Bell, J., Wagner, C., 2019: “Analysis of Model Mount Configurations with Regard to Force Measurements with Transient Inflow” New Results in Numerical and Experimental Fluid Mechanics XII, pp. 684-694

Prandtl L., 1914: "Der Luftwiderstand von Kugeln", Nachrichten von der Gesellschaft der Wissenschaften zu Göttingen, Issue 2, pp.177-190

Robinson, C., Baker, C., 1990: “The effect of atmospheric turbulence on trains”, J. Wind Eng. Ing. Aerodyn. 34:251-272

Rosa, L., Tomasini, G., Zasso, A., Aly, A.M., 2012: “Wind-induced dynamics and loads in a prismatic slender building: A modal approach based on unsteady pressure measurements”, j. Wind Eng. Ind. Aerodyn. 107-108 pp 118-130

Schröck, D., 2011: „Eine Methode zur Bestimmung der aerodynamischen Eigenschaften eines Fahrzeugs unter böigen Seitenwind“, PhD Thesis, Universität Stuttgart

Schröck, D., Wagner, A., 2013: “Aerodynamik und Fahrstabilität”. In: Schütz, T. (eds) Hucho - Aerodynamik des Automobils. ATZ/MTZ-Fachbuch. Springer Vieweg, Wiesbaden. https://doi.org/10.1007/978-3-8348-2316-8_5

Sears, W.R., 1941: “Some aspects of non-stationary airfoil theory and its practical application”, J. Aero. Sci, Vol. 8(3), pp. 104-108

Sterling, M., Baker, C., Boufferrouk, A., ONeil, H., Wood, S., Crosbie, E., 2009: “An investigation of the aerodynamic admittances and aerodynamic weighting functions of trains”, J. Wind Eng. Ing. Aerodyn. 97:512-522